

The influence of vegetation water dynamics on the ASCAT backscatter-incidence angle relationship in the Amazon

Ashwini Petchiappan¹, Susan C. Steele-Dunne², Mariette Vreugdenhil³, Sebastian Hahn³, Wolfgang Wagner³, and Rafael Oliveira⁴

¹Department of Water Management, Delft University of Technology, Stevinweg 1, Delft 2600 GA, The Netherlands

²Department of Geoscience and Remote Sensing, Delft University of Technology, Stevinweg 1, Delft 2600 GA, The Netherlands

³Department of Geodesy and Geo-Information, TU Wien, Vienna 1040, Austria

⁴Department of Plant Biology, Institute of Biology P.O.Box: 6109, University of Campinas – UNICAMP 13083-970, Campinas, SP, Brazil

Correspondence: Susan Steele-Dunne (s.c.steele-dunne@tudelft.nl)

1 **Abstract.** Microwave observations are sensitive to plant water content and could therefore provide essential information on
2 biomass and plant water status in ecological and agricultural applications. The combined data record of the C-band scatterom-
3 eters on ERS 1/2, the Metop series and the planned Metop Second Generation satellites will span over 40 years, which would
4 provide a long-term perspective on the role of vegetation in the climate system. Recent research has indicated that the unique
5 viewing geometry of ASCAT could be exploited to observe vegetation water dynamics. The incidence angle dependence of
6 backscatter can be described with a second order polynomial, the slope and curvature of which are related to vegetation. In a
7 study limited to grasslands, seasonal cycles, spatial patterns and interannual variability in the slope and curvature were found
8 to vary among grassland types and were attributed to differences in moisture availability, growing season length and pheno-
9 logical changes. To exploit ASCAT slope and curvature for global vegetation monitoring, their dynamics over a wider range
10 of vegetation types needs to be quantified and explained in terms of vegetation water dynamics. Here, we compare ASCAT
11 data with meteorological data and GRACE Equivalent Water Thickness (EWT) to explain the dynamics of ASCAT backscat-
12 ter, slope and curvature in terms of moisture availability and demand. We consider differences in the seasonal cycle, diurnal
13 differences, and the response to the 2010 and 2015 droughts across ecoregions in the Amazon basin and surroundings. Results
14 show that spatial and temporal patterns in backscatter reflect moisture availability indicated by GRACE EWT. Slope and cur-
15 vature dynamics vary considerably among the ecoregions. The evergreen forests, often used as a calibration target, exhibit very
16 stable behaviour even under drought conditions. The limited seasonal variation follows changes in the radiation cycle, and may
17 indicate phenological changes such as litterfall. In contrast, the diversity of land cover types within the Cerrado region results
18 in considerable heterogeneity in terms of the seasonal cycle and the influence of drought on both slope and curvature. Seasonal
19 flooding in forest and savanna areas also produced a distinctive signature in terms of the backscatter as a function of incidence
20 angle. This improved understanding of the incidence angle behaviour of backscatter increases our ability to interpret and make
21 optimal use of the ASCAT data record and ~~VOD~~ [Vegetation Optical Depth](#) products for vegetation monitoring.

22 1 Introduction

23 Microwave remote sensing observations are sensitive to plant water content, which depends on above ground biomass and plant
24 water status (Konings et al., 2019)(Konings et al., 2019; Owe et al., 2001; Jackson et al., 1982). Data from active and passive
25 microwave sensors can provide valuable information about vegetation in a range of applications in ecological and agricultural
26 monitoring (Konings et al., 2019; Steele-Dunne et al., 2017)(Konings et al., 2019; Chaparro et al., 2019; Rao et al., 2019; Steele-Dunne et
27 . In particular, Vegetation Optical Depth (VOD) products derived from various passive and active microwave sensors are in-
28 creasingly used for biomass monitoring (Liu et al., 2015), drought monitoring (Liu et al., 2018), wildfire risk assessment
29 (Forkel et al., 2019) and have been related to Gross Primary Production (Teubner et al., 2018, 2019), carbon stocks (Chaparro
30 et al., 2019) and drought-driven tree mortality (Rao et al., 2019). Currently VOD datasets are available from single sensor
31 passive microwave observations, such as SMAP (Konings et al., 2016), SMOS (Fernandez-Moran et al., 2017) and AMSR2
32 (Owe et al., 2001; De Jeu, 2003), and active microwave observations such as ASCAT (Vreugdenhil et al., 2016). Furthermore,
33 long-term data records are available that combine VOD from different sensors (Moesinger et al., 2020; Liu et al., 2011).

34 The current study is motivated by the availability of consistent C-band data from 1991 to at least 2030, and its potential
35 value as a long-term data record for vegetation monitoring. The Advanced Scatterometer (ASCAT) is a real aperture radar
36 operating at 5.255 GHz with VV polarization. There are currently three ASCAT instruments in orbit on Metop-A, Metop-B
37 and Metop-C, launched in October 2006, September 2012 and November 2018 respectively. ASCAT builds on the success
38 of the European Scatterometer (ESCAT) which flew on the ERS-1/2 satellites from 1991-2011 (Attema, 1991; Figa-Saldaña
39 et al., 2002; Wagner et al., 2013)). Continuation of the ESCAT/ASCAT record is ensured by the plans to launch SCA on
40 Metop-SG in 2024 (Stoffelen et al., 2017). Using data from a single series of satellites with identical and inter-calibrated
41 instruments circumvents many of the challenges of reconciling data using different frequencies, viewing geometries and orbit
42 characteristics. The continuity from ERS to Metop and Metop-SG ensures an internally consistent data product for at least 40
43 years, rendering it ideal to study the role of vegetation in the climate system.

44 Many early studies demonstrated the sensitivity of ESCAT and ASCAT backscatter to vegetation, and explored the potential
45 value of these data for vegetation monitoring (Wismann et al., 1995; Frison et al., 1998; Woodhouse et al., 1999; Jarlan et al.,
46 2002; Steele-Dunne et al., 2012; Schroeder et al., 2016). These studies focused on spatial and temporal variations in backscatter
47 normalized to some reference angle. Here, the focus is on the potential information content of the incidence angle behaviour
48 of backscatter, and particularly the so-called "Dynamic Vegetation Parameters" describing the incidence angle behaviour of
49 backscatter as calculated in the TU Wien Soil Moisture Retrieval (TUW SMR) algorithm (Hahn et al., 2017).

50 The ASCAT Dynamic Vegetation Parameters refer to the parameters of the second order Taylor polynomial used to describe
51 the incidence angle (θ) dependence of backscatter σ° . This is described as follows:

$$52 \quad \sigma^\circ(\theta) = \sigma^\circ(\theta_r) + \sigma'(\theta_r) \cdot (\theta - \theta_r) + \frac{1}{2} \cdot \sigma''(\theta_r) \cdot (\theta - \theta_r)^2 \quad [dB] \quad (1)$$

53 where $\sigma^\circ(\theta_r)$, $\sigma'(\theta_r)$ and $\sigma''(\theta_r)$ are the normalized backscatter, slope and curvature at some reference angle θ_r . In the TUW
54 SMR [algorithm](#), this expression is used to normalize backscatter values from different incidence angles to a reference angle

55 θ_r . It is also used to account for the influence of vegetation on backscatter as the incidence angle behaviour of σ° depends on
56 whether total backscatter is dominated by surface scattering from the soil, volume scattering from the vegetation, or multiple
57 scattering (Wagner et al., 1999; Naeimi et al., 2009; Hahn et al., 2017). In other words, slope and curvature are calculated
58 and used to account for the influence of vegetation in the soil moisture retrieval. An increase in soil moisture results in an
59 increase in backscatter at all incidence angles, while a change in the vegetation (due to growth cycle or water status) changes
60 the sensitivity of backscatter to incidence angle, i.e. it results in a change in slope and curvature. So, the slope and curvature
61 provide complementary information to the normalized backscatter.

62 Results from Steele-Dunne et al. (2019) suggest that considering the slope ($\sigma'(\theta)$) and curvature ($\sigma''(\theta)$) dynamics in com-
63 bination with the backscatter could yield valuable insights into vegetation water dynamics. Seasonal cycles, spatial patterns
64 and interannual variability in the slope varied between grassland cover type reflecting variations in soil moisture availability
65 and growing season length. Slope is considered an indication of vegetation density, or above ground fresh biomass, which is
66 a combination of dry biomass and vegetation water content. Results also suggested that curvature variations were influenced
67 by the total water content, but also its vertical distribution within the vegetation and the geometry of constituents. Contiguous
68 anomalies were observed in both slope and curvature during drought periods, suggesting that the slope and curvature provide
69 insight into when the severity of a soil moisture anomaly is enough to impact vegetation. Diurnal variations were also observed
70 and attributed to sub-daily variations in the dominant scattering mechanism due to changes in the vertical moisture distribution
71 of the grasses. More recently, Pfeil et al. (2020) observed a “spring peak” in slope values around April in broadleaf deciduous
72 forest in Europe. Using LAI and data from the Pan European Phenological database (PEP725) (Templ et al., 2018) they argued
73 that this spring peak in ASCAT slope coincides with spring activation, particularly the increase in water content of bare twigs
74 and branches prior to leaf out in broadleaf deciduous forests. ASCAT slope and curvature therefore seem to be sensitive to
75 changes in vegetation water content and structure of vegetation.

76 The goal of this study is to improve our understanding of the ASCAT backscatter-incidence angle relationship and how
77 they might be used to monitor vegetation water dynamics. The Amazon basin and its surroundings has been chosen as a study
78 area as it provides a wide range in terms of expected variability in ASCAT backscatter, slope and curvature. Backscatter in
79 the evergreen forest was considered so stable that this region has been used for satellite radar calibration (Birrer et al., 1982).
80 In contrast, seasonal changes in the Cerrado are expected to yield strong annual cycles in backscatter, slope and curvature.
81 Seasonal cycles and diurnal differences in ASCAT backscatter, slope and curvature will be determined for several ecoregions
82 of interest. These will be compared to meteorological data and GRACE terrestrial water storage variations to relate the ASCAT
83 backscatter, slope and curvature to moisture availability and demand. Finally, we will investigate whether there are anomalies
84 in the ASCAT backscatter, slope and curvature as a result of the 2010 and 2015 droughts.

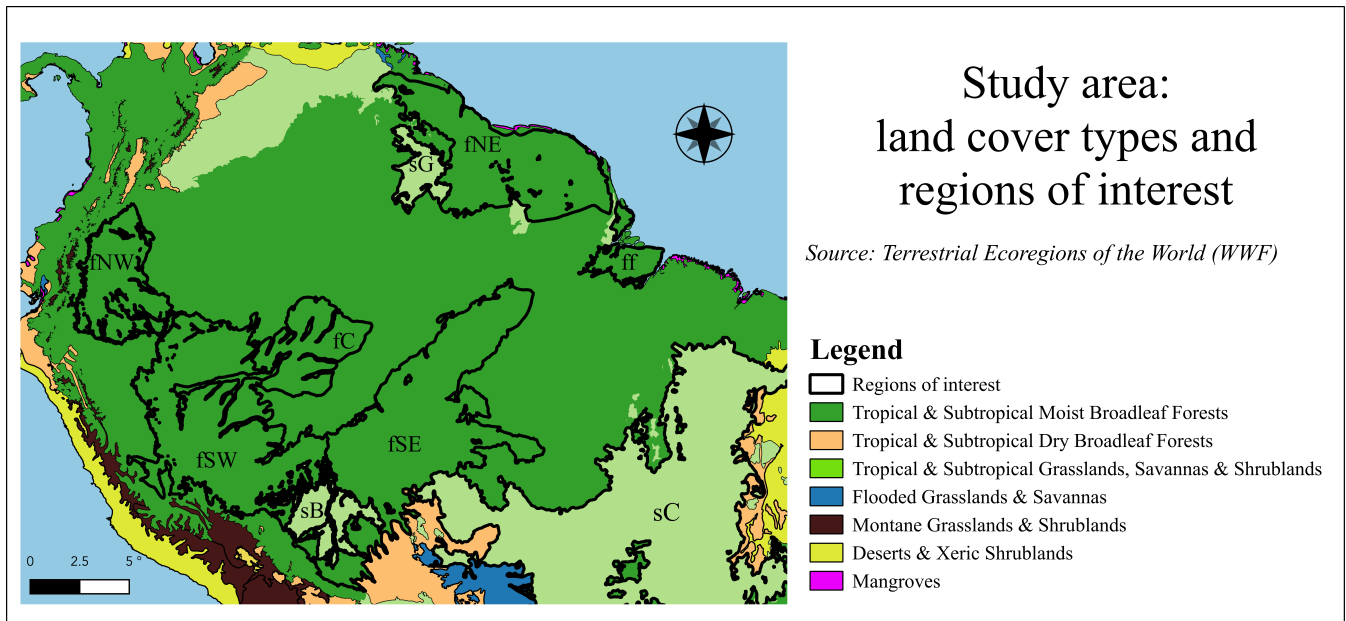


Figure 1. Study Area. The map is colored by biome, and nine ecoregions of interest are highlighted based on the dataset of Olson et al. (2001). The six forest ecoregions of interest are Napo moist forest (fNW), Guianan moist forests (fNE), Southwest Amazon moist forests (fSW), Madeira-Tapajos moist forest (fSE), Jurua-Perez moist forests (fC) and the Marajo Varzea flooded forests (ff). The three savanna ecoregions of interest are the Cerrado (sC), Guianan Savanna (sG) and Beni Savanna (sB).

85 2 Data and Methods

86 2.1 Study Area

87 Figure 1 shows the extent of the study domain, highlights the biomes (by color) and outlines the ecoregions of interest identified
 88 in the WWF Terrestrial Ecoregions dataset (WWF, 2019) and described by Olson et al. (2001). The study domain extends from
 89 9°N to 19°S, and 44°W to 80°W. Most of the study region is covered by the Amazon rain forest, which extends over 5.3
 90 million km² (Soares et al., 2006). Six forest ecoregions are investigated here:

- 91 1. The Napo moist forests (fNW), located in northwest Amazonia, receive some of the highest amounts of annual pre-
 92 cipitation in the biome, reaching up to 4000 mm in some parts. This highly biodiverse region has canopies reaching
 93 40 m.
- 94 2. The Guianan moist forests (fNE) are one of the largest continuous stretches of relatively pristine lowland tropical rain-
 95 forest in the world. There are two distinct wet seasons: from December to January and from May to August. The floral
 96 diversity is rich, with multi-tiered vegetation of 40 m tall trees with herbaceous plants below. The dry season (September-
 97 November) can see a substantial reduction in leaves, although the forest is evergreen.

- 98 3. The Southwest Amazon moist forests (fSW) have significant variations in topography and soil characteristics, leading
99 to extremely high biodiversity. The size and orientation of the ecoregion means that climatic conditions vary markedly
100 – the north being wetter and having less seasonal variability compared to the south. The inaccessibility of the region has
101 aided in its conservation.
- 102 4. The Madeira-Tapajós moist forests (fSE) are transected by the Transamazon Highway, and have high levels of urbaniza-
103 tion and deforestation. There are characteristic liana (woody vine) forests with a lower (< 25 m) and more open canopy
104 than the typical humid terra firme forests.
- 105 5. The Juruá-Perez moist forests (fC) are largely intact forests in the low Amazon Basin. The canopy can reach up to 30 m,
106 with some patches of open canopy.
- 107 6. The seasonally flooded forest, Marajó várzea (ff), is located at the mouth of the Amazon River. The vegetation is dom-
108 inated by palms, and shorter than surrounding forests. It has areas with tidal flows from the Atlantic Ocean, as well as
109 seasonally and permanently inundated forests. The annual seasonal flooding occurs during the peak precipitation period
110 between January-May (Camarão et al., 2002).

111 Three savanna ecoregions are also considered in this study:

- 112 1. The Cerrado (sC) borders the Amazon biome to the southeast. It occupies an area of 2 million km² in the Brazilian
113 Central Plateau and is the second most extensive biome in South America (Oliveira et al., 2005). The vegetation cover
114 varies from closed tree canopy to grasslands with low shrubs only (Eiten, 1972).
- 115 2. The Guianan savanna (sG) consists of forest patches encircled by extensive grasslands and shrub formations. The area
116 is more susceptible to vegetation fires than typical humid moist forest environments and the dry season lasts from
117 December-March.
- 118 3. The Beni savanna (sB) is a wetland region with riverine gallery forests and small forest islands. The landscape is domi-
119 nated by the palm species *Attalea princeps* (Hordijk et al., 2019). Seasonal flooding occurs in up to half the region for 4
120 to 9 months, peaking in March-April (Hamilton et al., 2004).

121 Three Köppen-Geiger Climate Classes (KGCC) cover most of the study region (Fig. 2). The evergreen forest regions are
122 classified as Af (tropical fully humid) or Am (tropical monsoonal), and the savanna regions have Aw (tropical winter dry)
123 climate (Bradley et al., 2011). The annual precipitation in the forests can exceed 2000-3000 mm, with less than 100 mm
124 rainfall for up to three months in the year. The savannas have a wet season extending for 5-8 months, with an annual total of
125 1000-2000 mm (Bradley et al., 2011). Net radiation peaks in the winter months, due to the absence of cloud cover in the dry
126 season (Liu et al., 2018). Two major droughts occurred in the region during the study period, in 2010 and 2015 (Jiménez-Muñoz
127 et al., 2016; Marengo et al., 2011) and are of particular interest in this study.

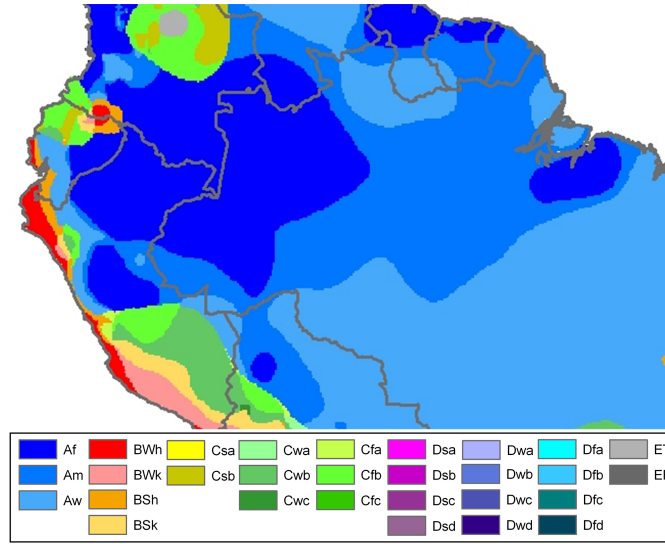


Figure 2. Köppen-Geiger climate zones in the study area (Source: (Peel et al., 2007)).

128 2.2 ASCAT data

129 The Advanced Scatterometer (ASCAT) data were processed using the same procedure as Steele-Dunne et al. (2019). Metop-A
 130 ASCAT SZR Level 1b Fundamental Climate Data Record, resampled at a 12.5 km swath grid, were obtained from the EU-
 131 METSAT Data Centre for the period 2007 to 2016. Following the procedure described by Naeimi et al. (2009), the backscatter
 132 observations were resampled to a fixed Earth grid using a Hamming window function. The slope and curvature were calculated
 133 from the ASCAT backscatter observations using the method introduced by Metzler (2013) and described by Hahn et al. (2017).
 134 The ASCAT instrument on-board the Metop satellites has three antennas on either side, oriented at 45° (fore), 90° (mid) and
 135 135° (aft) to the satellite track. As a result, three independent measurements of each location on the surface are obtained almost
 136 instantaneously. These so-called “backscatter triplets” (Hahn et al., 2017) are used to calculate an instantaneous backscatter
 137 slope, also known as the “local slope”:

$$138 \quad \sigma' \left(\frac{\theta_{mid} - \theta_{a/f}}{2} \right) = \frac{\sigma_{mid}^{\circ}(\theta_{mid}) - \sigma_{a/f}^{\circ}(\theta_{a/f})}{\theta_{mid} - (\theta_{a/f})} \quad [dB/deg] \quad (2)$$

139 where *mid*, *a* and *f* indicate the backscatter measurements from the mid-, aft- and fore-beams respectively. Following the
 140 approach of Metzler (2013), an Epanechnikov kernel (with width $\lambda=21$) is used to weight the local slope values by their
 141 temporal distance from a given day of interest. This yields an estimate of slope and curvature for a given day, based on all local
 142 slope values within a 42-day window. For a more detailed description of their derivation, the reader is referred to Steele-Dunne
 143 et al. (2019).

144 (Anderson et al., 2011) showed a calibration accuracy of Metop ASCAT backscatter of 0.15 - 0.25 dB. However, radiometric
 145 accuracy is expected to be better (i.e. less noisy) over stable, homogeneous targets (e.g. evergreen rainforest). To reduce

146 noise, the backscatter data is averaged in space (over the ecoregions of interest) and/or time (to monthly or dekadal intervals).
147 Observations from the descending and ascending overpasses are unlikely to occur on the same day. Hence, the σ_{40}° data were
148 aggregated into 10-day intervals (dekads). Unless otherwise indicated, the analysis uses data from the descending pass only (\sim
149 10 am). Diurnal differences refers to the values from the descending overpass (\sim 10 am) minus the values from the ascending
150 overpass (\sim 10 pm).

151 **2.3 Water Dynamics data**

152 Downwelling shortwave radiation at the surface and specific humidity were obtained from the Princeton meteorological dataset
153 (Sheffield et al., 2006). These data have a $0.5^{\circ} \times 0.5^{\circ}$ daily resolution. Precipitation data were obtained from the Global
154 Precipitation Climatology Product (GPCP) Precipitation Level 3 Monthly 0.5-Degree V3.0 beta dataset (Huffman et al., 2009).
155 Precipitation, radiation and humidity are hypothesized to be the main atmospheric forcing for vegetation activity in the Amazon
156 ((Nemani et al., 2003)). Therefore, these three forcings are compared to slope and curvature. As they are on similar temporal
157 and spatial scales, quantitative comparisons are performed. Data from the Gravity Recovery and Climate Experiment (GRACE)
158 mission were used to provide insight into terrestrial water storage variations (Landerer and Swenson, 2012; Swenson and Wahr,
159 2006). Here, we used the equivalent water thickness (EWT) from the GRACE Tellus dataset which is available at $1^{\circ} \times 1^{\circ}$,
160 monthly resolution from the NASA JPL Physical Oceanography Distributed Active Archive Center (PO DAAC). These data
161 give the relative change in EWT with respect to a baseline, the method of calculation for which is explained by Wahr et al.
162 (1998). These data provide information on fluctuations in EWT on monthly to inter-annual timescales. EWT includes variations
163 in all terrestrial water storage terms including groundwater, soil moisture, vegetation and surface water. Therefore, EWT is only
164 qualitatively compared to backscatter, which is affected by soil moisture and vegetation.

165 Seasonal cycles were determined for precipitation, radiation, humidity, and EWT by averaging data from the entire study
166 duration. Anomalies in precipitation during the drought years were also calculated (as drought year values minus climatology)
167 to provide an indicator of the water stress against which to compare the backscatter, slope and curvature anomalies.

168 **3 Results and Discussion**

169 **3.1 Seasonal Climatology**

170 Figure 3 shows the mean and range of normalized backscatter (σ_{40}°), slope and curvature for the study period (2007-16). In
171 general, the spatial patterns in the mean and range of all three quantities reflect the spatial patterns in land cover expected
172 from Fig. 1. It is striking that even the influence of the riverine network on the vegetation cover is discernible in the maps,
173 particularly that of the mean backscatter (Fig. 3(a)). Striping effects are visible in several of the maps, particularly that of the
174 range in curvature (Fig. 3(f)). This is due to the backscatter observations at the swath edges being available only at very high
175 or very low incidence angles, which skews the calculation of the slope and curvature. This effect is particularly noticeable in
176 forest regions where the natural dynamic range in both quantities is limited.

177 Mean backscatter is highest, with the least variability, in the evergreen forest regions ~~-(Fig.A1)~~. Mean backscatter is 2-
178 2.5 dB lower in the savanna areas, but the range is up to 3 dB, compared to just 0.5 to 1 dB in the forest. The stability of
179 the forest is also apparent in the maps of slope and curvature. Though there is some variability among the forest ecoregions,
180 the most striking differences in slope and curvature are between the forest and savanna areas. Limited structural and water
181 content changes in the forest canopy result in a limited range of slope and curvature values in the forest ecoregions. The range
182 of both slope and curvature are highest in the Cerrado areas ~~-(Fig.A1)~~. One interesting feature is the difference in mean slope
183 between the Guianan savanna (sG) in the north and the Cerrado (sC) region in the south. The Guianan savanna, with sparse
184 vegetation, has low mean slope values. The Cerrado, on the other hand, shows mean values higher than the evergreen forests.
185 This is unexpected since slope is generally considered a measure of “vegetation density”, and the evergreen forests are much
186 denser than savannas. This will be discussed in detail in Sect. 3.1.1. Seasonal flooding of the Marajó várzea (the seasonally
187 flooded forest) and Beni savannas ensure that both ecoregions have strong seasonal cycles in all three quantities. These will be
188 discussed separately in Sect. 3.1.2.

189 The mean seasonal cycles in backscatter for ~~the-all~~ ecoregions of interest are compared in Fig. 4 (a). This highlights the
190 contrast between the very stable evergreen forest regions and the flooded forest and savanna areas. The mean backscatter value
191 is high, with limited seasonal amplitude in the evergreen forest regions. Backscatter variations are so limited in these areas that
192 they have long been used as calibration targets for spaceborne radar (Birrer et al., 1982; Kennett and Li, 1989; Frison and Mougin, 1996; H
193 . In contrast, backscatter is generally low, but also exhibits strong seasonal variations in the flooded forest and savanna areas.
194 Figures 4 (b-f) show the seasonal variation in backscatter split out for five ecoregions of interest, against the correspond-
195 ing climatologies of precipitation and EWT. As the evergreen forest ecoregions showed very similar climatologies, only the
196 Jurua-Purus moist forest is shown as a separate plot. In all of the ecoregions, the maximum backscatter occurs during the
197 wet season, and a decrease in backscatter is observed during the dry season, though the amplitude of the variations is ob-
198 viously much smaller in the forest ecoregions. In each ecoregion, there is clear agreement between the seasonality of EWT
199 and backscatter. This indicates that backscatter is influenced by moisture availability in terms of total terrestrial water storage,
200 which includes groundwater storage. It is noteworthy that this temporal consistency between backscatter and EWT is apparent
201 for both forest (fC in Fig. 4 (b)) and the Guianan Savanna (sG in 4 (e)) despite the contrast between almost zero (0.25 dB)
202 variability in backscatter in fC and the 2.5 dB seasonal cycle in sG. Figure A2 shows temporal correlation between backscatter
203 and precipitation is low for all ecoregions. A strong negative correlation and strong positive correlation are found with radiation
204 and humidity for lags between -2 and 2 months, indicating that backscatter is lowest during drier periods with higher radiation
205 and lower specific humidity.

206 Figure 5 (a) summarizes the mean seasonal cycle in the slope for the ecoregions of interest. The difference between ecore-
207 gions is more pronounced than for backscatter. The seasonal cycle for the evergreen forest ecoregions are similar in magnitude
208 but there are minor differences in the timing of the peak. The differences between the savanna regions are more pronounced
209 than for backscatter. Significant differences can be seen in the mean slope value, as well as the amplitude and timing of the
210 seasonal cycle of slope values for each ecoregion of interest.

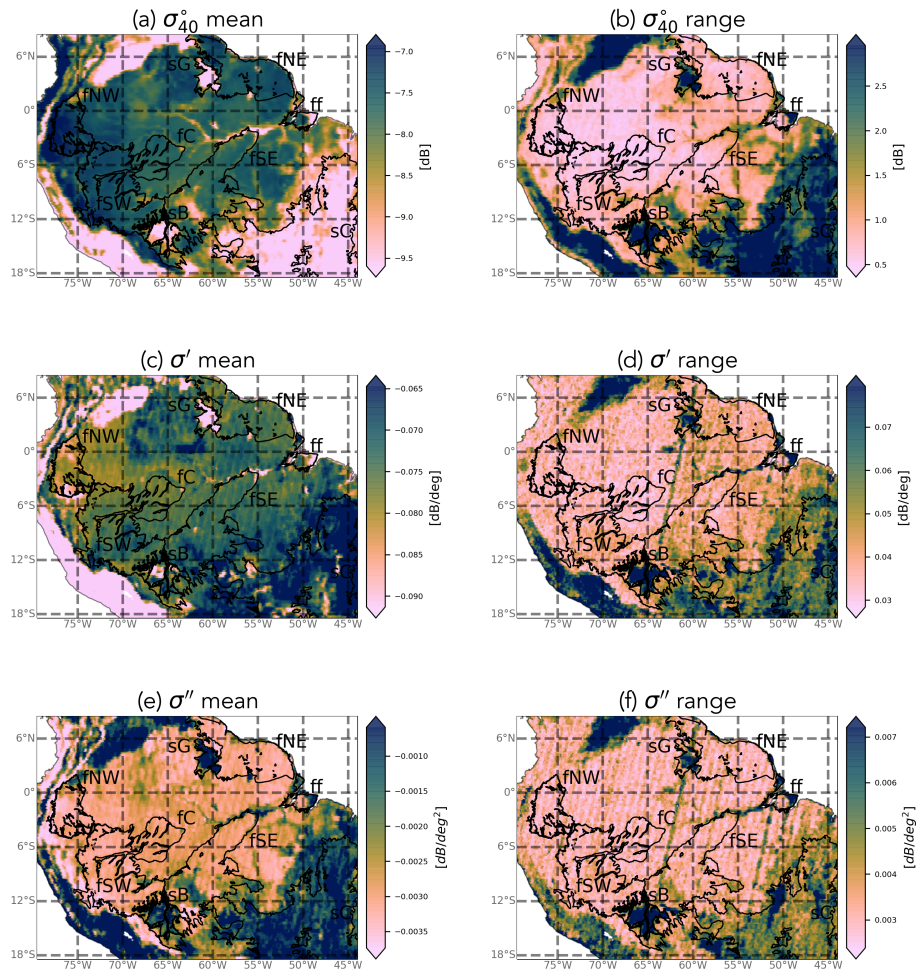


Figure 3. Mean and range of ASCAT normalized backscatter, slope and curvature in the study period (2007-16). Note that there are no data gaps, so white indicates that the quantity has a value equal to or less than the minimum value indicated on the colorbar.

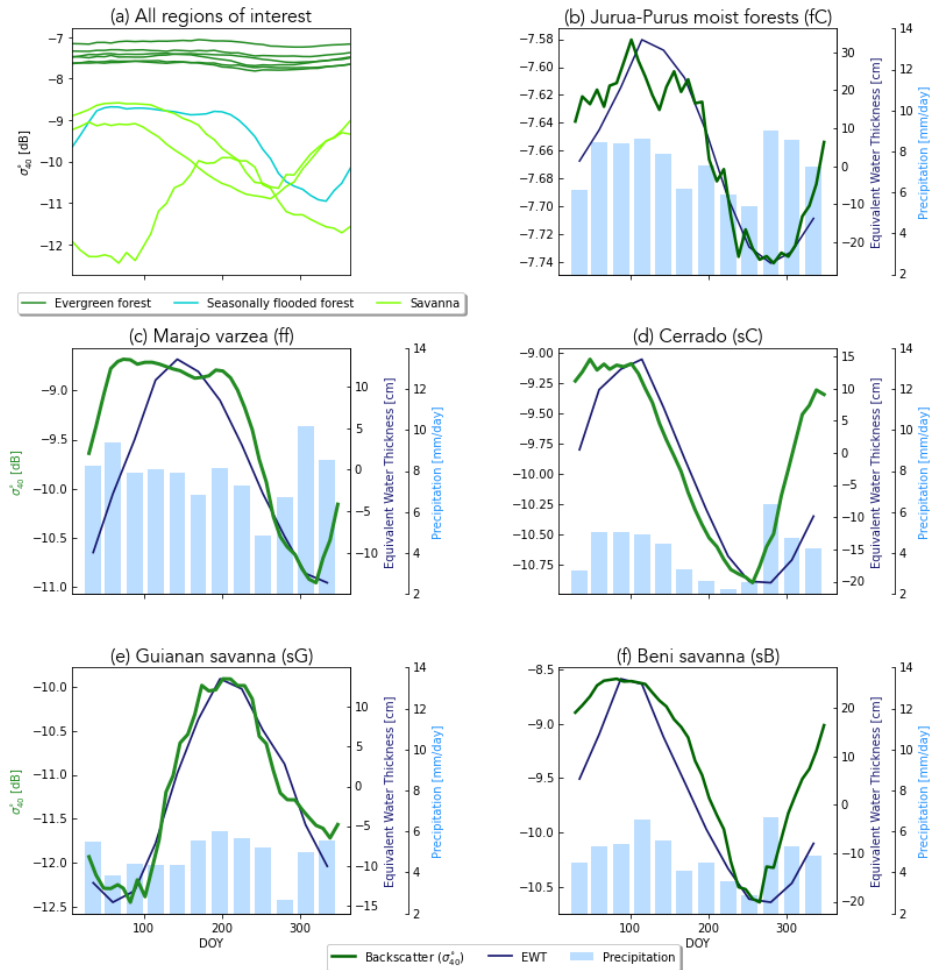


Figure 4. Climatology of backscatter for all ecoregions; five evergreen forest (dark green line), flooded forest (cyan) and three savanna (light green) (a). Plot (b) to (f) show climatology of backscatter (green line) with precipitation (bars) and EWT (blue line) for per ecoregion. Note the different cover types axes and that only the Jurua-Purus moist forest (fC) is shown as it is similar to the other evergreen forests.

211 In Fig. 5(b-e-b-f), the seasonal cycle of slope in each ecoregion is compared to the corresponding cycles of radiation, specific
212 humidity and precipitation which drive photosynthetic activity in the region. Note again that only the Jurua-Purus moist forest
213 is shown as a separate plot. Furthermore, Fig. A2 illustrates the temporal correlation between slope and precipitation, radiation
214 and specific humidity. In the Jurua-Purus moist forests (Fig. 5(b)), the change in slope is one-tenth that observed in the other
215 ecoregions. The variations in radiation and specific humidity are also very limited. Nonetheless, the seasonal cycle of the
216 slope follows that of the radiation with a lag of about 30 days -(Fig. A2, R=0.75 at lag -1). This can be explained by the fact
217 that the vegetation phenology in this tropical evergreen forest is driven by radiation (Romatschke and Houze Jr, 2013). The
218 photosynthetic capacity depends on the available solar energy (Borchert et al., 2015). Energy availability drives transpiration
219 and the accumulation of leafy biomass. This increases volume scattering from the canopy and therefore leads to an increase
220 in the slope. Similar results were observed for the other forest ecoregions. In the Marajo varzea flooded forest (Fig. 5(c)), the
221 variation in slope is much larger, and the seasonal cycle is clearly out of phase with that of the radiation. The seasonal variations
222 in slope in this ecoregion are dominated by the influence of surface flooding rather than vegetation water content variations
223 (Sect. 3.1.2).

224 In the Cerrado (Fig. 5(d)), there is a significant variation in specific humidity, and radiation as well as a strong seasonal cycle
225 in precipitation. The peak in slope occurs during the driest time of year, when radiation is at a maximum and specific humidity
226 and precipitation are at a minimum. Recall from Fig. 4, that this is also during the minimum EWT and backscatter period. This
227 is also illustrated in Fig.A2 where strong negative correlations are found between slope and humidity. Correlations between
228 slope and radiation are lower, and the highest correlation occurs at a lag of two months, i.e. slope leads radiation. Section
229 3.1.1 provides a detailed analysis of the vegetation types within the Cerrado ecoregion to better understand these variations.
230 The slope values in the Guianan Savanna (Fig. 5(e)) are the lowest observed in all ecoregions, and also have the smallest
231 variations among the non-forest cover types which are not strongly related to precipitation, radiation or specific humidity. This
232 is consistent with the relatively low, but stable vegetation density associated with grasslands (Steele-Dunne et al., 2019). In
233 the Beni Savanna (Fig. 5(f)), on the other hand, slope varies as much as in the Cerrado, and there is a very clear relationship
234 between the slope and the atmospheric forcing data (Fig. 5 (f)). The maximum slope occurs at the peak of precipitation, EWT
235 (from Fig. 4) and humidity. The minimum slope occurs during the dry season at the minimum in precipitation, humidity and
236 EWT. This is consistent with the interpretation of slope as an indicator of vegetation density as the vegetation cover in this
237 savanna changes dramatically in response to atmospheric forcing. This is also illustrated in Fig.A2, where high correlations are
238 observed between slope and humidity with small lags. The contrast in the seasonal cycles in slope in Fig. 5 reflect the diversity
239 of the vegetation cover types in the ecoregions and their varied response to moisture supply and demand.

240 Figure 6 (a) shows the mean seasonal cycles in curvature for the regions of interest. The differences in the amplitudes of the
241 seasonal cycles vary considerably among the regions. While the evergreen forests vary less than 0.0005 dB/deg^2 , variations
242 in the wetland regions (Beni savanna and Marajó várzea) are an order of magnitude larger. Aside from the Guianan savanna,
243 the timing of the seasonal cycle is similar across all ecoregions. Previous research has suggested that curvature is related
244 to vegetation phenology and structure (Steele-Dunne et al., 2019). Since the vegetation phenology in much of the forested
245 region is radiation-driven, we hypothesize that the curvature seasonality is related to the radiation and evaporative demand.

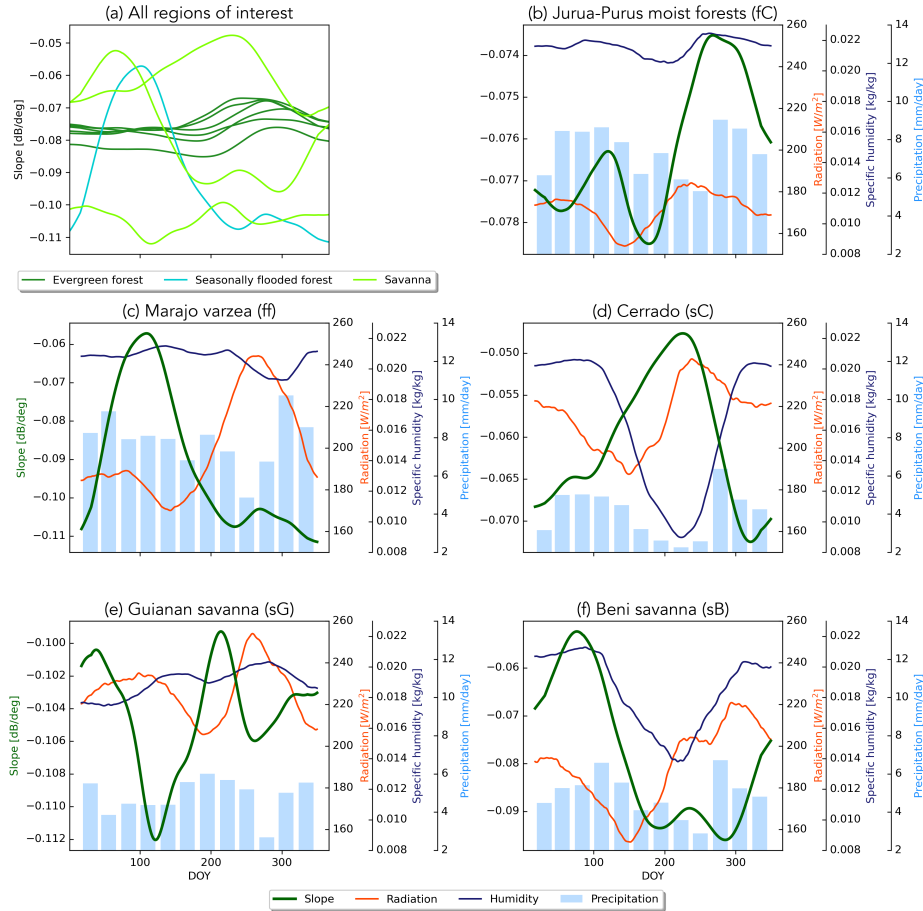


Figure 5. Climatology Climatologies of slope for all ecoregions; five evergreen forest (dark green line), radiation-flooded forest (red-cyan) and three savanna (light green) (a). Plot (b) to (f) show climatology of slope (green line) with precipitation (bars) and specific humidity (blue line) and precipitation-radiation (bars red line) for per ecoregion. Note the different cover types axes and that only the Jurua-Purus moist forest (fC) is shown as it is similar to the other evergreen forests.

246 ~~Wagner et al. (2016) observed that litterfall coincides with maximum evaporative demand, which would coincide with lower~~
247 ~~humidity and higher solar radiation. Leaf flushing is induced by an increase in radiation (Borchert et al., 2015)~~In the Amazon
248 rainforest, Borchert et al. (2015) observed that leaf flushing and flowering in adult trees of numerous species coincided with
249 the rise and decline of insolation. Wagner et al. (2016) made a similar observation about leaf flushing and rising insolation in
250 July, and also noted that the litterfall peak occurs when evaporative demand is highest and can persist through the dry season.
251 Figure 6 (b) shows that although the changes in curvature are very small in the rainforest, the peak occurs in July on the rising
252 limb of the radiation data, and when the specific humidity is near its minimum. Figures 6 (b-f) demonstrate that higher and Fig.
253 A2 show the strong correspondence between curvature and radiation (positive correlation at a lag of 2 months) and specific
254 humidity (negative correlation with a lag of -1 month) and that the highest values of curvature generally correspond to lower
255 humidity, higher solar radiation and lower precipitation. This suggests that higher values of curvature may be related to litterfall
256 during periods of high evaporative demand. It is also noteworthy that the curvature values in the Guianan savanna (Fig. 6 (e))
257 are positive for much of the year, consistent with the dominance of grass cover in this region.

258 3.1.1 Cerrado

259 As described in Section 3, the Cerrado shows a peak in slope, which indicates increased volume scattering, at a time of low
260 precipitation and humidity, maximum radiation and low backscatter. To better understand these variations backscatter, slope
261 and curvature are analyzed per land cover class. Figure 7 provides a detailed map of the Copernicus Global Land Service
262 Land Cover within the Cerrado region Buchhorn et al. (2020). The dominant cover types are herbaceous cover and shrubland,
263 with patches of cropland and forest. Figures 8 and 9 show the spatial patterns and boxplot per land cover type of mean,
264 maximum and the DOY of the maximum for backscatter, slope and curvature. The mean backscatter varies between -13 and
265 -7 dB and is highest for forest regions and lowest for croplands. The DOY for the maximum backscatter varies with latitude,
266 from December to January in the southern region to April in the northern region. ~~The~~ As expected, the highest backscatter
267 corresponds with the months of highest precipitation and EWT, the minimum in backscatter corresponds with the months of
268 lowest moisture availability (Fig. 4). The seasonal dynamics in backscatter are strongest in cropland. This may be related to the
269 higher sensitivity to surface soil moisture in croplands and low backscatter may be related to dry surface soil conditions. The
270 slope mean and maximum values show a decrease from shrubs to herbaceous to cropland, decreasing with vegetation density as
271 expected. Forests are characterised by high mean and maximum slope values. The seasonal dynamics and DOY of the maximum
272 slope vary strongly with land cover type. In croplands, the maximum ~~of slopes~~ slope, i.e. where volume scattering is highest,
273 occurs between DOY 340-150, corresponding. This corresponds to the highest precipitation and EWT, indicating increased
274 vegetation density. In natural vegetation, such as herbaceous cover, shrubs and forests, the highest slope occurs between day
275 200 and 300 and coincides with the minimum in precipitation and EWT ~~and but with~~ maximum radiation (Fig. 5). ~~Within the~~
276 ~~Cerrado region, vegetation can be moisture limited or energy limited (Nemani et al., 2003), depending on location and land~~
277 ~~cover type. This is illustrated in~~ Figure 10 ~~shows the, where~~ slope and radiation dynamics for different land cover classes are
278 depicted. To exclude confounding effects due to heterogeneous land cover within ASCAT pixels, we used only pixels with a
279 dominant land cover fraction of > 80%. The slope dynamics in cropland are following the precipitation dynamics and have their

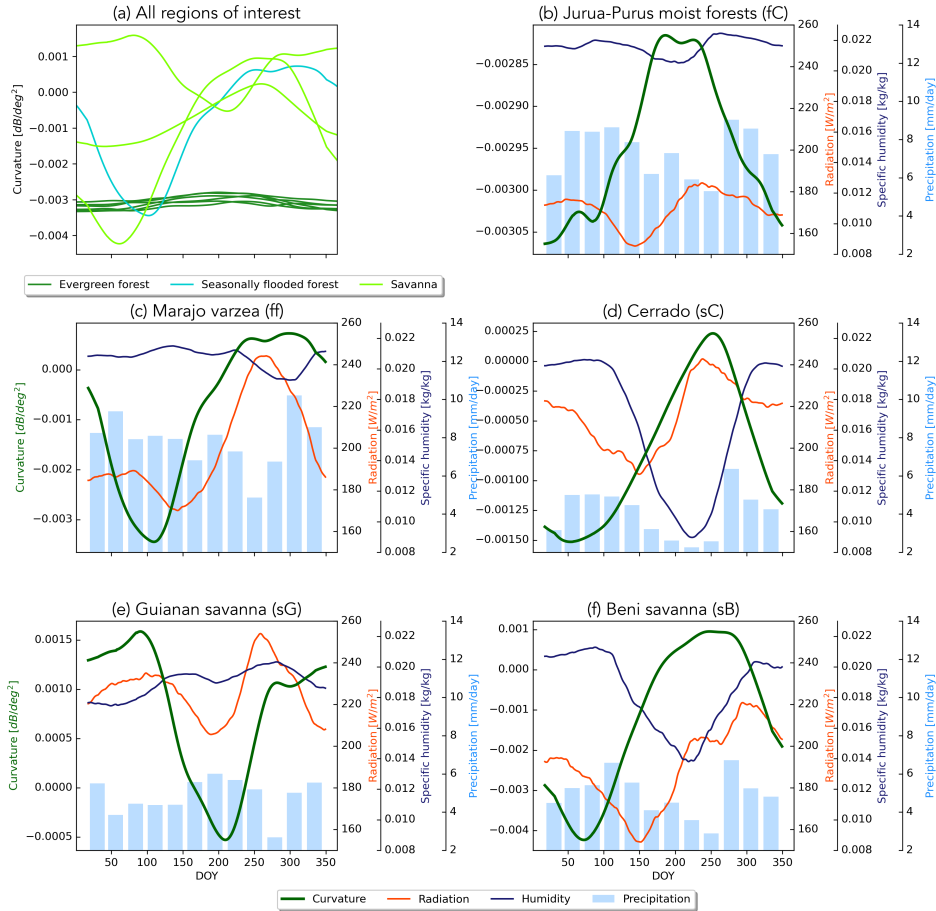


Figure 6. Climatology–Climatologies of curvature for all ecoregions: five evergreen forest (dark green line), radiation–flooded forest (red cyan) and three savanna (light green) (a). Plot (b) to (f) show climatology of curvature (green line) with precipitation (bars) and specific humidity (blue line) and precipitation–radiation (bars red line) for per ecoregion. Note the different y-axes and that only the Jurua-Purus moist forest (fC) is shown as it is similar to the other evergreen forests.

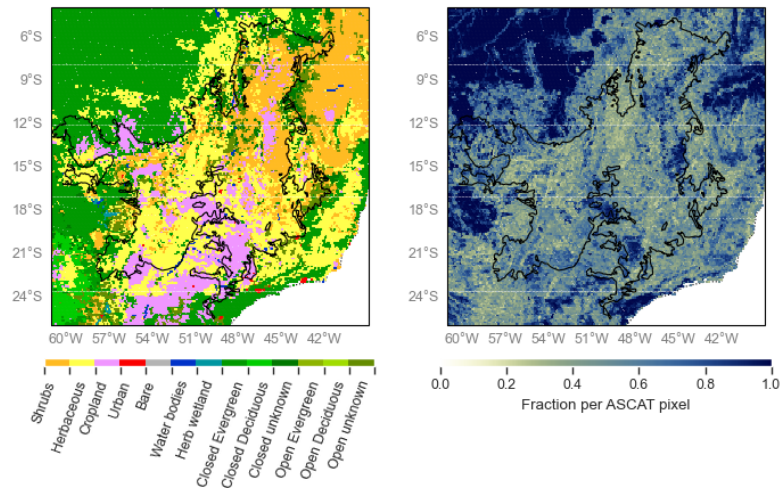


Figure 7. Dominant land cover type (left) and fraction (right) derived from the Copernicus Global Land Service Land Cover (2015) for the Cerrado region Buchhorn et al. (2020)

280 peak during the wet season. Herbaceous cover shows two peaks in slope, one coinciding with the wet season at the beginning
 281 of the year, and a higher peak coinciding with the dry season and maximum in radiation. The increase in slope coincides
 282 with the onset of the increase in radiation. In shrubs and forests, slope starts to increase after the wet season, but before the
 283 increase in radiation (Fig. 10). Shrubs and This counter-intuitive behavior of the slope over natural vegetation can be explained
 284 by the variability in limiting factors to vegetation activity. Within the Cerrado region, vegetation can be moisture limited or
 285 energy limited (Nemani et al., 2003), depending on location and land cover type. Contrary to crops, natural vegetation types
 286 such as herbaceous vegetation, shrublands and forests have deeper root systems and they can tap into deeper water reservoirs.
 287 This enables them to increase photosynthesis and leaf development slightly before or at the onset of increasing radiation even
 288 though precipitation is at its minimum. The increase in vegetation activity will lead to increased volume scattering and a flatter
 289 backscatter over all incidence angle and subsequent higher slope. Chave et al. (2010) found that, among the tropical forest
 290 types in South America, the highest seasonality in litterfall was observed in "low" stature forests, such as those found in the
 291 Cerrado. They also cite Wright and Van Schaik (1994) to argue that seasonality of solar radiation rather than precipitation
 292 may be the most important trigger for leaf flushing and leaf abeissionabscission. Croplands and herbaceous vegetation show
 293 positive curvatures, whereas forests are characterised by negative curvatures with the maximum values occurring between DOY
 294 200 and 300 across the Cerrado. The positive curvature for crops and herbaceous vegetation can be explained by the vertical
 295 structure of the vegetation.

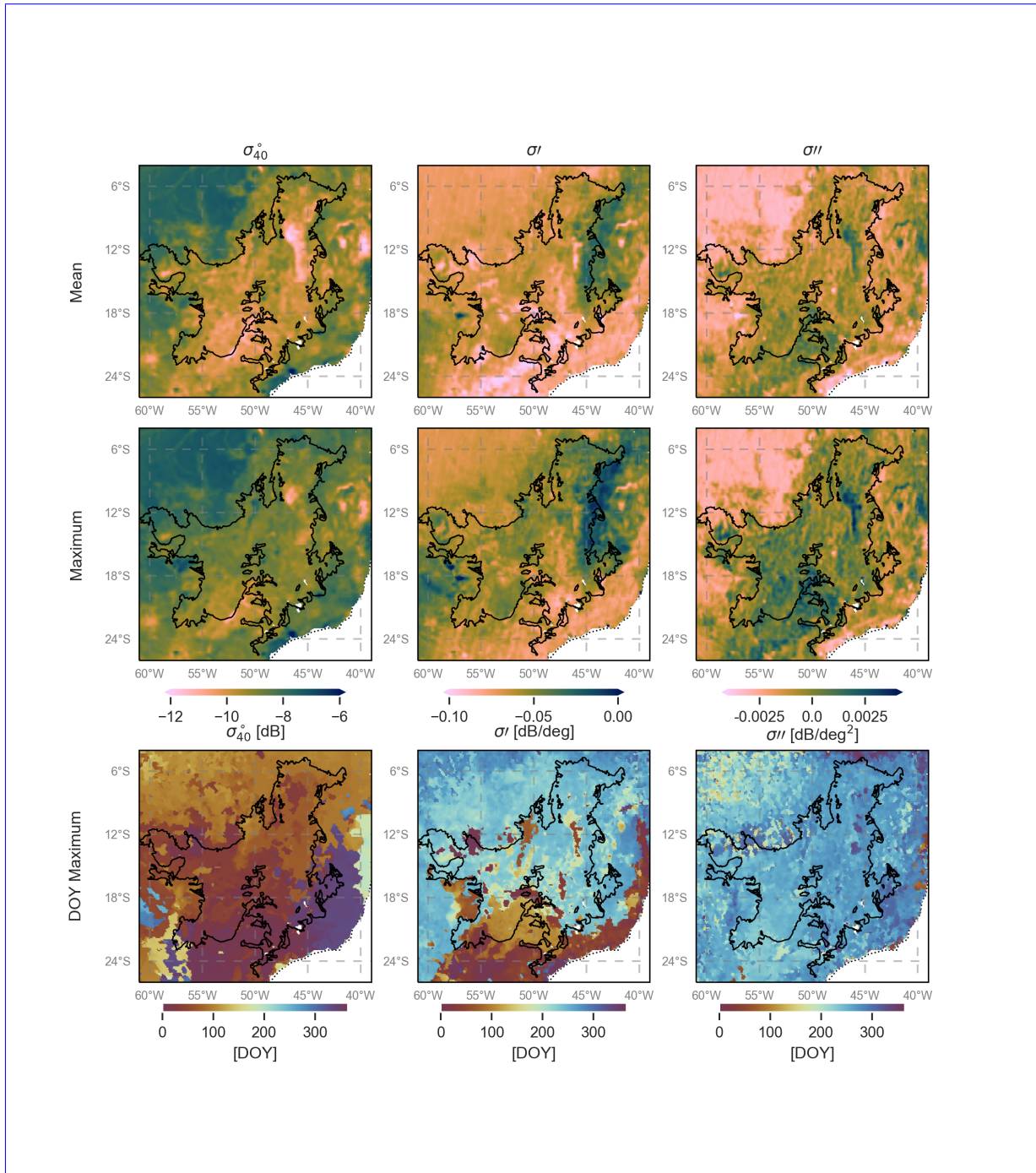


Figure 8. Mean, maximum and day of year of maximum for backscatter, slope and curvature over the Cerrado.

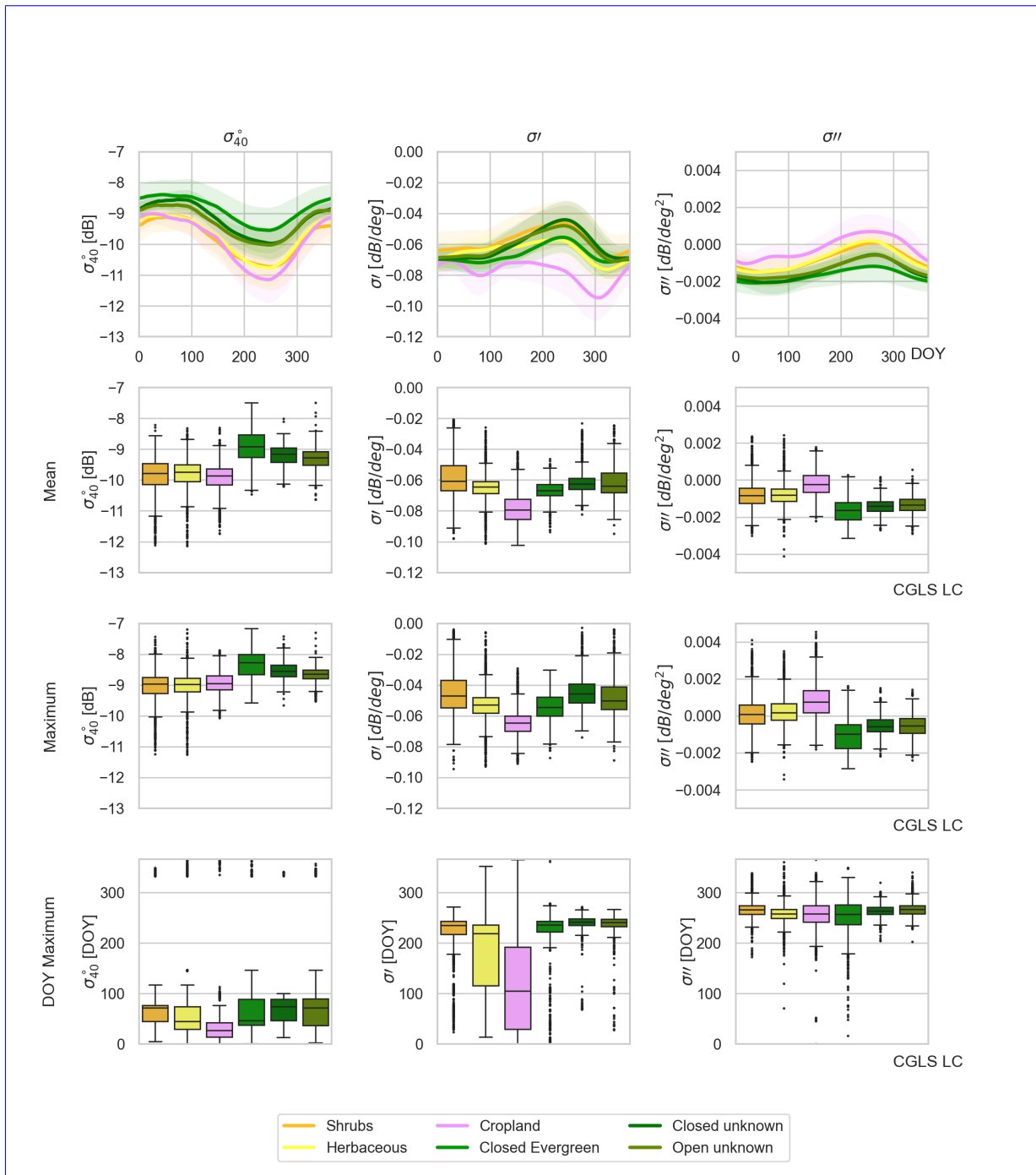


Figure 9. Time series averaged per land cover class and boxplots of mean, maximum and day of year of maximum for backscatter, slope and curvature over the Cerrado.

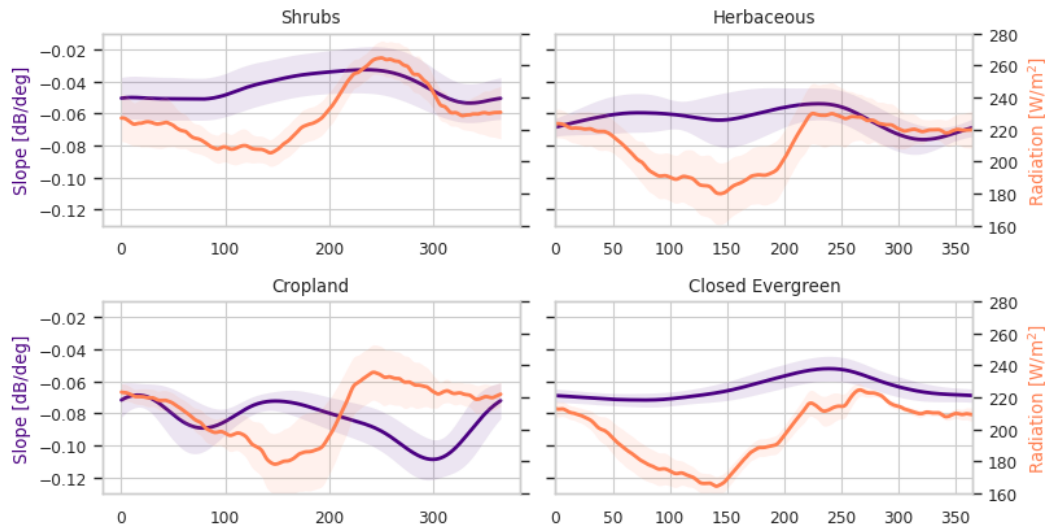


Figure 10. Seasonal cycle of slope and radiation per land cover class in the Cerrado region. Only ASCAT pixels in which the fraction of the dominant land cover type exceeds 80% are included.

296 3.1.2 Seasonal Flooding

297 Fig. 11 shows the striking effect of seasonal flooding on the incidence angle dependence of backscatter. This relationship was
 298 obtained using Equation 1 for a reference angle of 40° with the climatological mean values of σ_{40}° , slope and curvature for
 299 several days during the year. The flooded period is indicated in shades of blue. First, note that σ_{40}° is around 2 dB higher
 300 during the seasonal flooding. ~~This~~ Under forest/woody vegetation, this is due to ~~multiple~~ a combination of double bounce
 301 ~~scattering between the water surface and the vegetation.~~ surface and trunks, and multi-path scattering between the surface and
 302 the vegetation (Townsend, 2002).

303 Recall from Fig. 5 that the slope is slightly higher during this period as this multiple scattering is apparently slightly less
 304 sensitive to incidence angle than scattering from the vegetation during non-flooded period. However, the most noteworthy
 305 difference is in the curvature. In both ecoregions, the curvature changes considerably and even changes sign during the flooded
 306 period. This illustrates that the curvature includes useful information on changes in the scattering mechanisms, which are
 307 related to physical changes at the land surface.

308 3.2 Diurnal Differences

309 Figure 12 shows the mean diurnal differences for backscatter and EWT in the study area for alternate months in the year,
 310 where positive values indicate that values are higher during the descending (10 am) overpass than those from the ascending
 311 (10 pm) overpass. The diurnal differences in backscatter are generally very small, with maximum values less than 0.15 dB.
 312 ~~Nonetheless,~~ Although this is unquestionably close to the limits of the ASCAT sensor in terms of radiometric accuracy, these

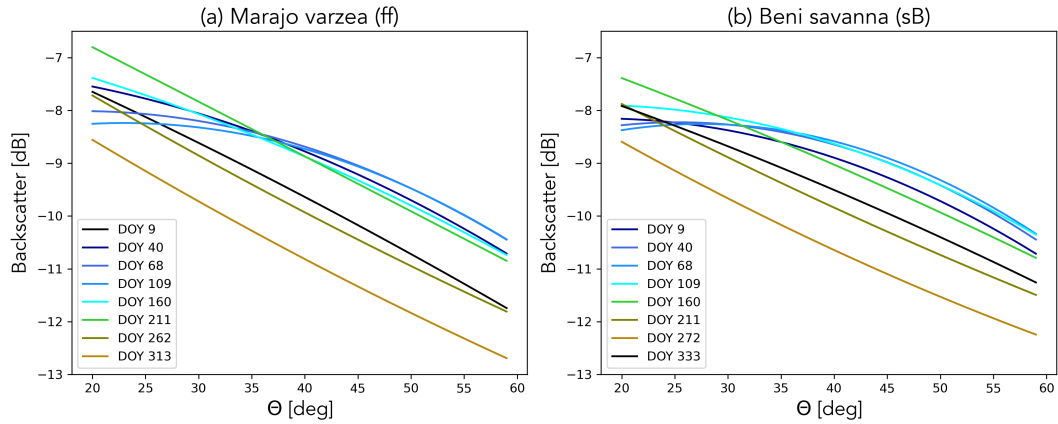


Figure 11. Averaged backscatter as a function of incidence angle for several dates in the Marajo varzea (a) and Beni Savanna (b) ecoregions.

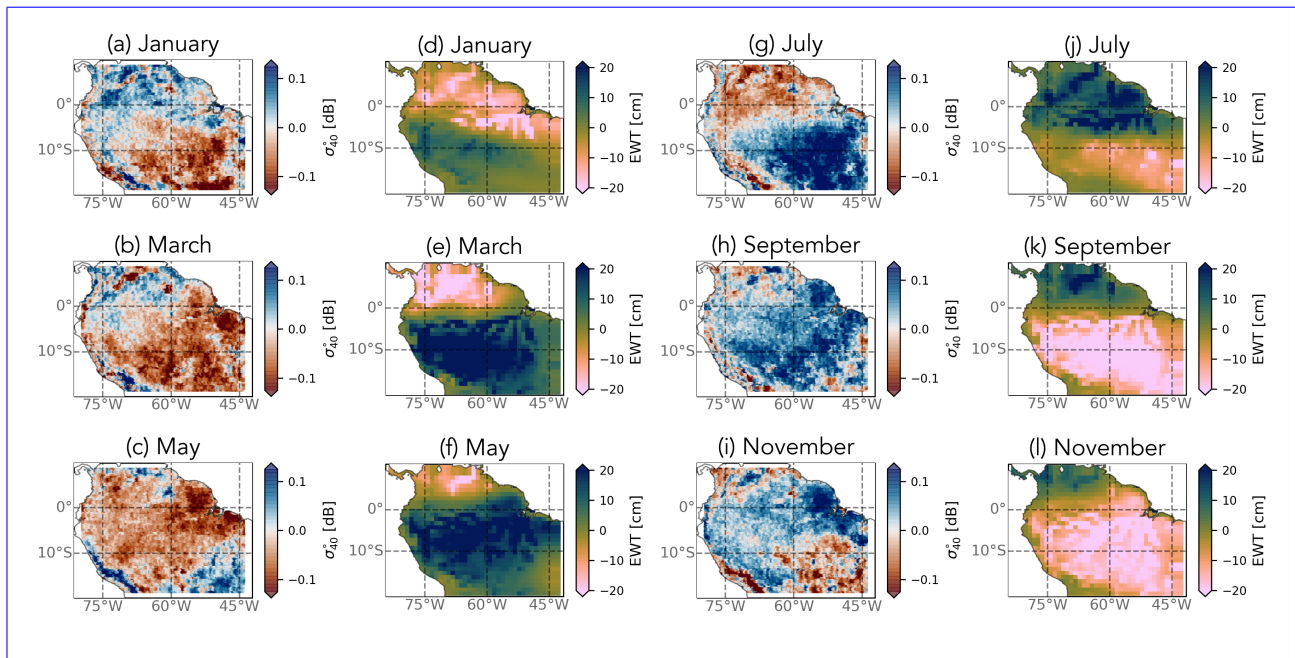


Figure 12. Map Maps of monthly mean diurnal differences in σ_{40}° (morning minus evening passes) and monthly mean Equivalent Water Thickness (EWT) from GRACE for different months in the year.

313 results are based on monthly averages, which is expected to reduce noise. Furthermore, there is a clear seasonal variation,
 314 broadly following that of EWT (shown in Fig. ??), demonstrating that patterns are likely not a result of noise.

315 Map of monthly mean Equivalent Water Thickness from GRACE

316 For most of the domain, especially the evergreen forests, high values in EWT coincide with negative diurnal differences in
317 backscatter and vice versa. During periods of maximum EWT, the backscatter is higher in the evening than in the morning.
318 This is consistent with the finding that precipitation in tropical South America (since it is generally produced by convective
319 systems) predominantly occurs in the late afternoons and evenings (Romatschke and Houze Jr, 2013). Hence, these higher
320 backscatter values are due to the canopy being wetter in the evening.

321 During the drier periods (e.g. September (eh, k) and November (fi, l) in the south of the study area), backscatter is higher at
322 10 am than at 10 pm, consistent with the loss of moisture through transpiration during the day. In a light-limited evergreen forest
323 such as the Amazon (rather than a water-limited forest), the canopy photosynthetic capacity seasonality is driven by radiation
324 (Wagner et al., 2016). When the plants are phenologically active, they lose water during the daytime through transpiration
325 resulting in lower evening backscatter values. The results in Fig. 12 and ?? are consistent with the findings of previous studies
326 by Frohling et al. (2011) and Friesen et al. (2012) who also found the morning backscatter over Amazonia to be higher (on
327 average) than the evening values due to higher water content in the vegetation. In the areas surrounding the evergreen forests,
328 the patterns can be less straight-forward. Note, for example, that the diurnal difference in σ_{40}° in the Guianan savanna (sG)
329 consistently has the opposite sign to that of the surrounding forest.

330 In Fig. 13, the seasonal cycle of the diurnal difference in σ_{40}° is compared to those of the radiation, precipitation and EWT
331 for each of the ecoregions of interest. Figure 13(a) is indicative of the seasonal variations observed across the evergreen forest
332 ecoregions. Note that the diurnal differences are very small (< 0.06 dB). Recall from Fig. 4, 5 and 6 that the backscatter, slope
333 and curvature in these evergreen forests was essentially stable throughout the year, so even this small diurnal difference is
334 noteworthy given the limited seasonal variation. As mentioned in the discussion of Fig. 12, evening values are higher than
335 morning values during the EWT maximum and vice versa. Diurnal differences are larger in the Marajo varzea (Fig. 13(b)), but
336 interpreting their seasonal variation is complicated by the seasonal inundation. In the Cerrado and Beni Savanna ecoregions
337 (Fig. 13(c) and (e)), the diurnal differences in backscatter are almost twice as large as those observed in the evergreen forest
338 regions. Morning values are up to 0.1 dB higher than evening values during the dry season due to loss of plant moisture during
339 the day. Similar to the forest regions, evening backscatter values are higher during the rainy season. The Guianan savanna
340 (Fig. 13(d)) is quite distinct in that morning backscatter is up to 0.15 dB higher than evening backscatter during the EWT
341 and backscatter peak. One possible explanation for this unusual seasonal cycle is that it is related to a change in the relative
342 dominance of the forests and grasslands in the backscatter signal. The transition from positive to negative curvature values
343 during the EWT peak indicate an increased contribution from tree patches and shrubs during the wetter period. The higher
344 backscatter in the morning may be due to water uptake in the trees during the night.

345 3.3 The 2010 and 2015 droughts

346 During the study period (2007-16), two major droughts occurred in Amazonia, in 2010 and 2015. Figure 14 shows the spatial
347 distribution of anomalies in σ_{40}° , slope and curvature during the peak of the droughts from June to September 2010 and October
348 to December 2015. Two regions of interest are indicated in the maps, the savanna Cerrado (sC) ecoregion and Southwest
349 Amazon moist forests (fsW). The 2010 drought was most severe over southern and western Amazonia (Panisset et al., 2018).

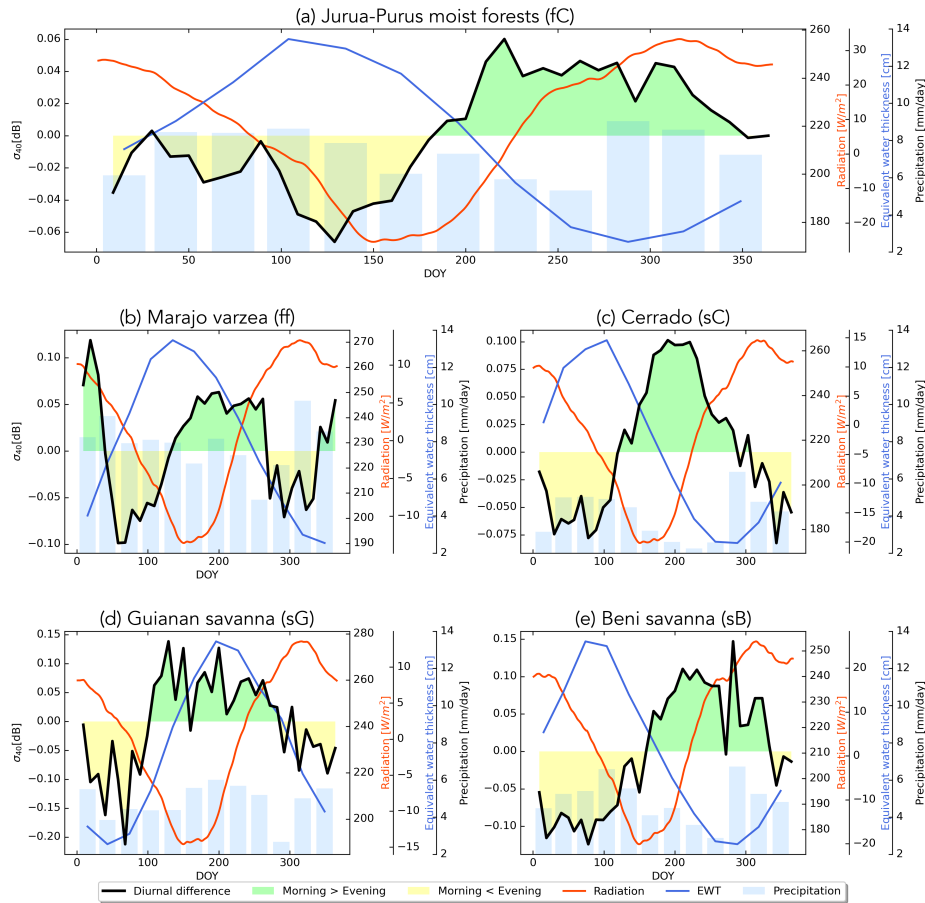


Figure 13. Seasonal cycle of diurnal difference in backscatter (black line), radiation (red line), EWT (blue line), and precipitation (bars) for different cover types. Green (yellow) fill indicates days in which backscatter is higher (lower) in the morning than in the evening.

350 The 2015 drought was considered a “record-breaking” event with stronger warming than that seen in previous events (Jiménez-
 351 Muñoz et al., 2016). According to Panisset et al. (2018), there was a “pronounced lack of rainfall availability during late spring
 352 and early summer”. The 2015 drought was more widespread than the event in 2010, and strongest in eastern Amazonia.

353 Negative anomalies are observed in σ_{40}° , especially in the southern regions and in the Cerrado in 2010 and in eastern regions
 354 in 2015. Note that the most eastern part of the Cerrado shows positive anomalies in 2010. The forests in fsW show minor
 355 negative anomalies (<0.1 dB) in σ_{40}° in 2010 and slightly stronger negative anomalies in 2015. Negative anomalies in backscat-
 356 ter from QSCAT were also observed during the 2005 drought (Saatchi et al. (2013); Frohling et al. (2017)). No significant
 357 spatial or temporal anomalies were observed in the diurnal differences in backscatter during the drought years. The slope and
 358 curvature do not show clear spatial patterns in anomalies during the 2010 drought, although the southern region shows slightly

359 more positive anomalies. A clear positive anomaly can be observed in the slope in eastern Amazonia in the 2015 drought. The
360 curvature shows less clear patterns, although a striping pattern can be seen, likely related to swaths.

361 Figure 15 shows the time series of anomalies in backscatter, slope and curvature for the moist forests in fsW and the Cerrado
362 region for the 2010 and 2015 drought. The backscatter, slope and curvature over the closed evergreen forest in fsW shows very
363 little variation (both in time and space) during both droughts. A slight increase up to 0.002 dB/deg in slope can be observed
364 during the peak of the 2015 drought. This demonstrates that the fsW forests are stable for satellite calibration. The Cerrado
365 shows varying responses depending on land cover type and are therefore investigated further. Negative anomalies in σ_{40}° in
366 cropland and herbaceous land cover can be seen during both droughts. Especially during the 2010 drought the croplands in the
367 Cerrado are strongly affected, with a negative anomaly of $>-1\text{dB}$ for some pixels. During the more extensive drought in 2015,
368 σ_{40}° in forest is also affected and negative anomalies up to -1.5 dB are observed. The slope shows minor positive anomalies
369 during the peak of the drought in 2010. In an analysis of drought impact on VOD over the forests in southern Amazonia,
370 Liu et al. observed similar positive anomalies in VOD from May to August during the 2010 drought. Negative anomalies in
371 VOD were only observed during later stages of the drought, from August to October. In 2010, negative slope anomalies in
372 the Cerrado are observed from October on. During the 2015 drought strong positive anomalies in slope and curvature are
373 present over the Cerrado especially in forests. Contrary to the drought of 2010, the peak of the 2015 drought occurs during
374 the precipitation season in the Cerrado. Normally the precipitation season is characterised by lower radiation, and the positive
375 anomalies in radiation during the drought might enhance vegetation growth.

376 4 Conclusions

377 In this study, ASCAT backscatter, slope and curvature were analyzed in conjunction with meteorological data and terrestrial
378 water storage from GRACE in the Amazon region. Previous results, limited to grasslands, had suggested that the slope and
379 curvature contained useful information for monitoring vegetation water dynamics. However, the current study is the first to
380 ~~relate attempt to explain~~ the spatial and temporal variations in slope and curvature ~~to~~ in terms of seasonal variations in moisture
381 availability and demand. Furthermore, it confirms that the conclusions of Steele-Dunne et al. (2019) can be extended to a wide
382 range of cover types.

383 Results show that the unique viewing geometry of ASCAT provides valuable insight into vegetation water dynamics across
384 a diverse range of ecoregions. ~~Strong temporal consistency was found between ASCAT backscatter and~~ The timing of the
385 seasonal cycle of normalized backscatter was consistent with that of GRACE EWT, with the maximum (minimum) normalized
386 backscatter coinciding with ~~periods of maximum moisture availability~~ the maximum (minimum) EWT in all ecoregions. Spatial
387 patterns in mean and range of slope ~~reflected spatial patterns in vegetation density~~ reflect the ecoregions within the study area.
388 The seasonal cycle in slope was found to follow the moisture availability and demand indicated by meteorological data and
389 their influence on phenology. A detailed analysis per land cover type over the Cerrado demonstrated this. Slope dynamics
390 were concurrent with precipitation in croplands and herbaceous cover, although herbaceous cover showed a second peak
391 coinciding with the maximum in radiation. Slope dynamics in shrubs and forest corresponded with radiation, although the

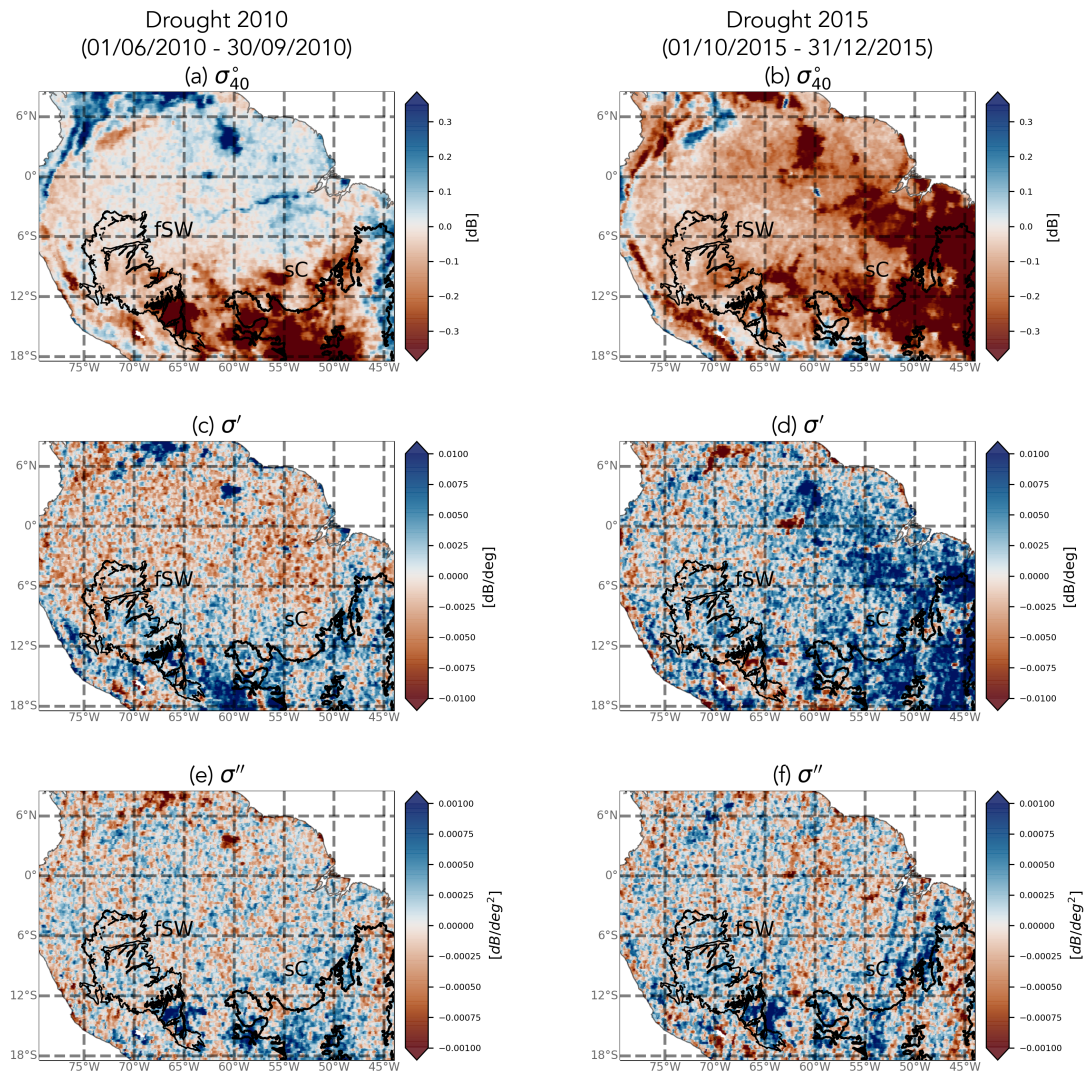


Figure 14. Spatial patterns in anomalies in backscatter, slope and curvature in response to the 2010 and 2015 droughts.

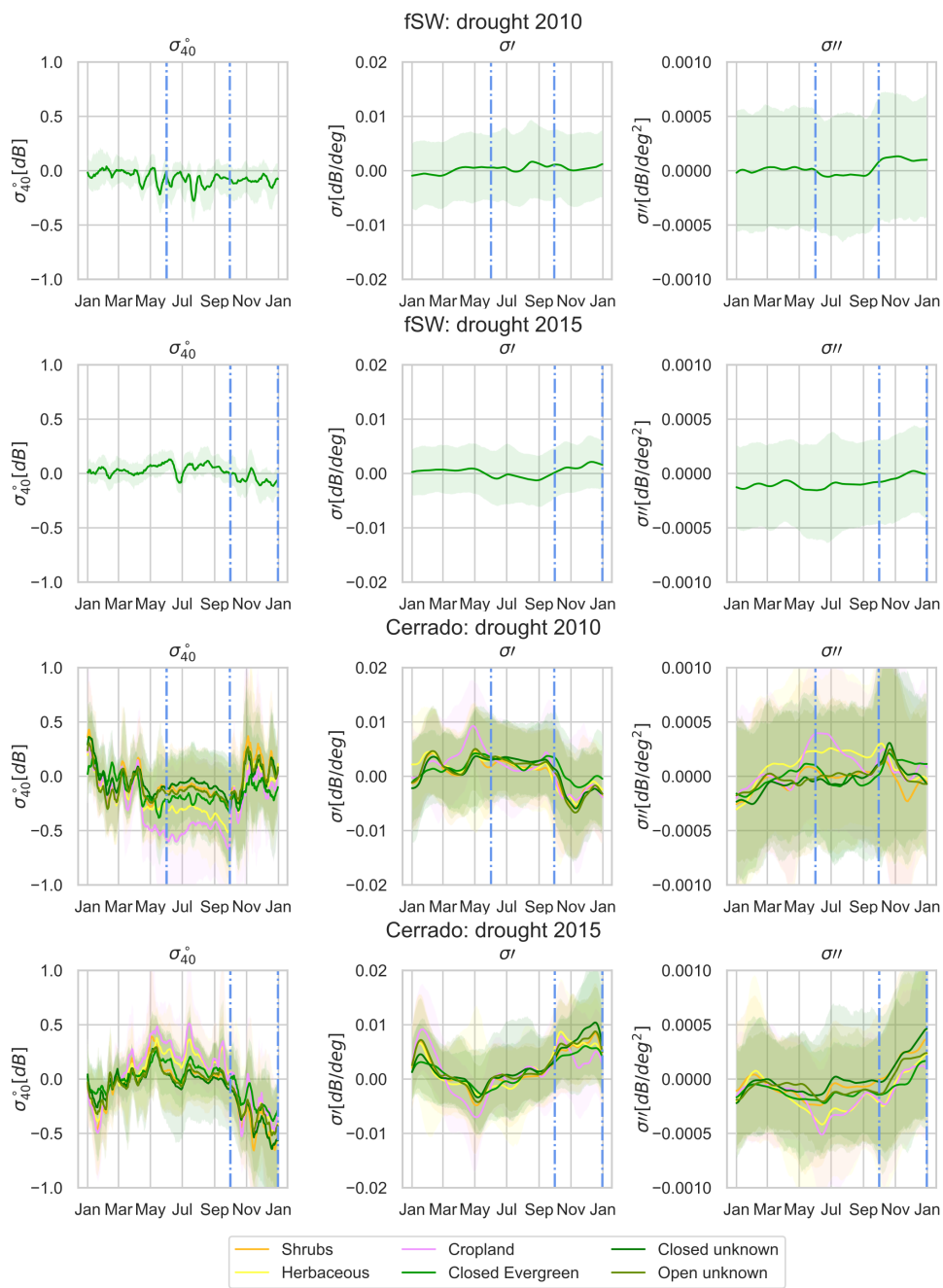


Figure 15. Time series of anomalies in backscatter, slope and curvature for moist forest (fsW) and Cerrado region. The shaded areas indicate the 5th and 95th percentile. The peak drought intervals (June-September 2010 and September-December 2015) are shown within **dotted dashed-dotted** blue lines.

392 onset in increasing slope preceded the onset of increasing radiation. This may be due to leaf flushing, but it is difficult to draw
393 a firmer conclusion given the limited availability of ground data ~~Chave et al. (2010)~~ [\(Chave et al., 2010\)](#). While the mechanism
394 driving these variations in slope may not be immediately clear, it is important to note that there are open questions around
395 the process of litterfall and its relation to precipitation and radiation in general. A recent study from Hashimoto et al. (2021)
396 demonstrated that the temporal density of optical data from the Advanced Baseline Imager (ABI) onboard the Geostationary
397 Operational Environmental Satellite 16 (GOES-16) yields unprecedented detail on the seasonality of NDVI and LAI in the
398 evergreen Amazon forests. A comparison of ASCAT slope and curvature and ABI data may yield additional insight into the
399 connection between slope, curvature and litterfall in the various ecoregions of our study area. Consistent with the findings
400 of Steele-Dunne et al. (2019) in a study limited to grasslands, variations in curvature seem to be related to phenological
401 change. ~~Temporal consistency between the curvature and meteorological data suggests sensitivity to events such as litterfall~~
402 ~~and~~ [The highest values of curvature coincide with periods of high evaporative demand \(e.g. high radiation, lower humidity and](#)
403 [lower precipitation\). This suggests a link between curvature and phenological changes such as leaf flushing and litterfall. For](#)
404 [example, the curvature peak in July in the rainforest occurs during rising insolation, and coincides with](#) leaf flushing. Areas
405 affected by seasonal flooding exhibited dramatic changes in both backscatter and curvature due to a suspected increase in
406 multiple scattering between water on the surface and the vegetation.

407 Diurnal variations (i.e. the difference between morning and evening overpasses) were generally small, particularly in the
408 evergreen forests. Nonetheless, their relation to the timing of precipitation highlights the importance of overpass time in using
409 microwave observations for vegetation monitoring. Diurnal differences in backscatter during the dry season are dominated by
410 transpiration losses. Long-term monitoring of these diurnal differences could provide insight into moisture availability and its
411 influence on transpiration and vegetation functioning [\(Konings et al., 2021\)](#). Consistent with previous studies on the effect of
412 drought on the backscatter signal over the Amazon forests (Frolking et al., 2011; Saatchi et al., 2013), a negative anomaly in
413 backscatter was observed during the 2010 and 2015 drought, although this was minor for the moist forests, strong anomalies
414 were observed in the Cerrado. The slope showed positive anomalies during the drought events in the Cerrado, similar to
415 positive anomalies in VOD over forests observed by Liu et al. who attributed this to enhanced canopy growth due to increased
416 radiation. Persistent positive anomalies in radiation were observed over the Cerrado, especially in 2015. The analysis confirms
417 the confounding effects of mechanisms driving variation in slope in these regions ~~and further research is needed~~.

418 ~~This~~ [The](#) improved understanding of slope and curvature [gained in this study](#) is valuable in terms of our ability to use
419 ASCAT for vegetation monitoring, and specifically for vegetation water dynamics. The slope and curvature are used to produce
420 the ~~vegetation optical depth~~ [VOD](#) from ASCAT (Vreugdenhil et al., 2016). ~~Improved~~ [Our improved](#) understanding of the
421 slope and curvature and how they are affected by vegetation structure and water content, and interactions between the soil
422 and vegetation is essential to improve our ability to interpret and optimally use VOD derived from ASCAT. [Therefore, this](#)
423 [research contributes directly to the continued development of the ASCAT VOD products](#). Furthermore, the fact that the slope
424 and curvature themselves reveal different aspects of the vegetation response to the balance between moisture availability
425 and demand means they are potentially useful low-level observables, i.e. they are obtained with minimal processing, and
426 avoid the assumptions and simplifications required to retrieve geophysical variables. The results of this study suggest that

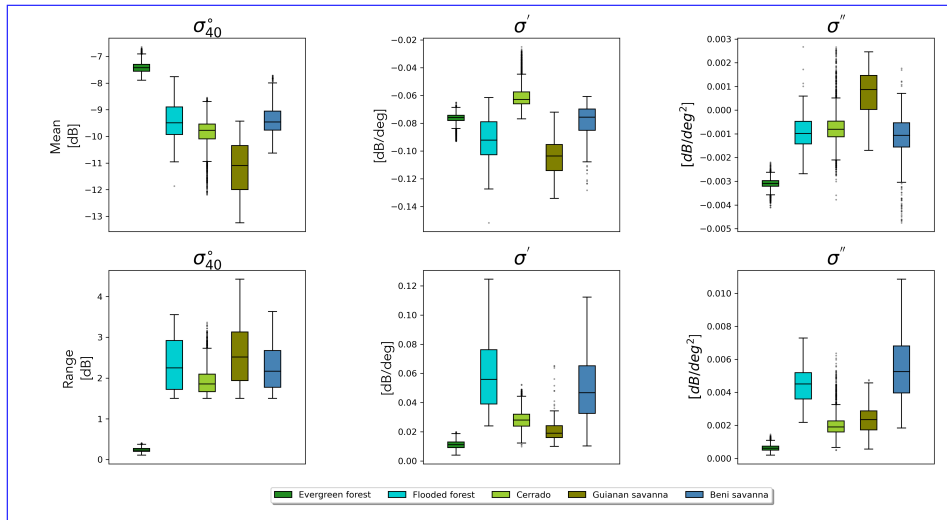


Figure A1. Mean (top row) and range (bottom row) for backscatter, slope and curvature for different ecoregions.

427 their information content can be directly exploited to monitor vegetation water dynamics. The current study was performed
 428 over different land cover types, demonstrating the potential to study vegetation water dynamics with these observables over
 429 different regions. However this research also confirms the need for further research to overcome the limited understanding of
 430 the spatio-temporal dynamics of slope compared to environmental drivers and effects in structure of vegetation. A lot of our
 431 understanding of the incidence angle dependence of backscatter is based on experiments with tower-based or airborne radar
 432 systems conducted in the 1970s to 1990s (e.g. Ulaby (1975); Ferrazzoli et al. (1992)) to optimize the design of spaceborne
 433 radar systems. However, these experiments were generally focused on classification, soil moisture or LAI/biomass retrieval.
 434 Radar data were limited in space and/or time, and water dynamics (beyond soil moisture) were often not considered. Recent
 435 studies have focused on the relation between water dynamics in vegetation and tower-based radar backscatter response(e.g.
 436 (Vermunt et al., 2020; Khabbazan et al., 2022)), but not at the slope of the backscatter incidence angle relationship. So, in any
 437 first-order ground validation, we advocate the inclusion of incidence angle dependence. Nonetheless, field-based experimental
 438 campaigns have the disadvantage that they are very localized. Thus, studies like the one presented here, to explore ASCAT
 439 dynamic vegetation parameters and explain the variations in terms of modeled or observed geophysical variables are equally
 440 valuable and needed, because they allow us to study a wide range of cover and climate types and the impact of events such
 441 as drought. Based on this, and considering the planned SCA instrument on Metop-SG, incidence angle variations should be
 442 studied in more detail and be considered as a potentially valuable source of useful information. Ongoing research is focused
 443 on using data-driven and radiative transfer modeling approaches to investigate the sensitivity of slope and curvature to physical
 444 changes at the land surface including also different regions and cover types.

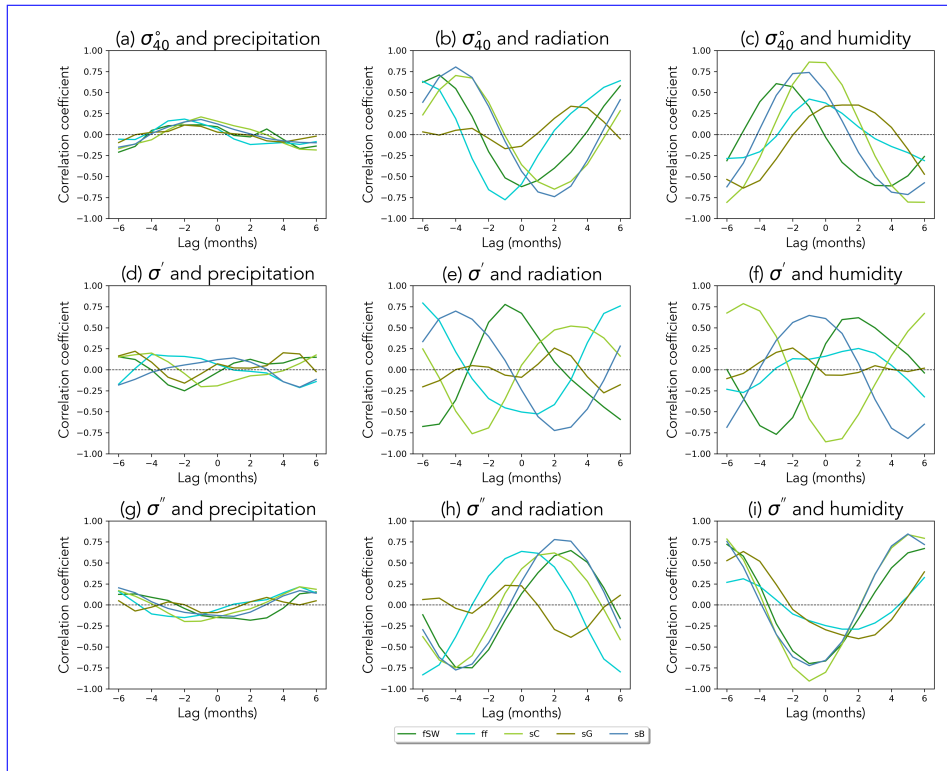


Figure A2. Correlation between backscatter (top row), slope (middle row) and curvature (bottom row) with precipitation, radiation and humidity for the different ecoregions for different lag times.

445 *Author contributions.* AP, SSD and MV were responsible for the conceptualization, methodology, formal analysis, investigation, visual-
 446 ization and writing (original draft preparation). SH provided resources (ASCAT data). RO contributed to the investigation. SSD and MV
 447 provided supervision. All authors contributed to writing (review and editing).

448 *Competing interests.* The authors declare that no competing interests are present.

449 *Acknowledgements.* Susan Steele-Dunne was supported by ~~Vidi Grant 14126 from~~ The Netherlands Organization for Scientific Research
 450 (NWO) - User Support Programme Space Research (Project ALWGO.2018.036 - 'A new perspective on global vegetation water dynamics
 451 from radar satellite data') and NWO Vidi Grant 14126. Mariette Vreugdenhil was supported by ESA's Living Planet Fellowship SHRED
 452 (contract number 4000125441/18/I-NS).

